Langmuir

ARTICLE

pubs.acs.org/Langmuir

UPS, XPS, and NEXAFS Study of Self-Assembly of Standing 1,4-Benzenedimethanethiol SAMs on Gold

Luca Pasquali,[†,§] Fabio Terzi,[‡] Renato Seeber,[‡] Stefano Nannarone,[†,§] Debasish Datta,[∥,⊥,#] Céline Dablemont,[⊥,#] Hicham Hamoudi,[⊥,#] Maurizio Canepa,[▽] and Vladimir A. Esaulov*[,⊥,#]

[†]Dipartimento di Ingegneria dei Materiali e dell'Ambiente, Università di Modena e Reggio Emilia, Via Vignolese 905, 41100 Modena, Italy

[‡]Dipartimento di Chimica, Università di Modena e Reggio Emilia, Via Campi 183, 41100 Modena, Italy

[§]CNR-IOM, s.s.14, km 163.5 in Area Science Park, 34012 Trieste, Italy

[∥]Seth Anandram Jaipuria College, 10, Raja Naba Krishna Street, Kolkata 700 005, India

[⊥]Université-Paris Sud, Institut des Sciences Moléculaires d'Orsay, Orsay, France

[#]CNRS, UMR 8214 Institut des Sciences Moléculaires d'Orsay, ISMO, Bâtiment 351, UPS-11, 91405 Orsay, France

[▽]CNISM and Dipartimento di Fisica, Università di Genova, Via Dodecaneso 33, 16146 Genova, Italy

ABSTRACT:

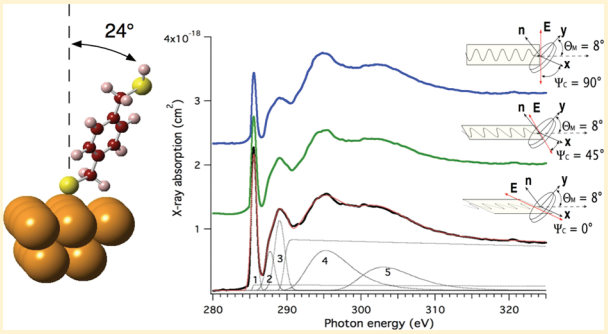

We report a study of the self-assembly of 1,4-benzenedimethanethiol monolayers on gold formed in n-hexane solution held at 60 °C for 30 min and in dark conditions. The valence band characteristics, the thickness of the layer, and the orientation of the molecules were analyzed at a synchrotron using high resolution photoelectron spectroscopy and near edge X-ray adsorption spectroscopy. These measurements unambiguously attest the formation of a single layer with molecules arranged in the upright position and presenting a free −SH group at the outer interface. Near edge X-ray absorption fine structure (NEXAFS) measurements suggest that the molecular axis is oriented at 24° with respect to the surface normal. In addition, valence band features could be successfully associated to specific molecular orbital contributions thanks to the comparison with theoretically calculated density of states projected on the different molecular units.

INTRODUCTION

Dithiol molecules, in particular, molecules containing aromatic rings, have been the object of much investigation because of potential use in, for example, molecular electronics thanks to their conducting properties and the possibility to graft the thiol ends to two metal electrodes.[1−7] Furthermore, dithiol molecules self-assembled on surfaces can, under suitable conditions, bond to the surface with one −SH group, while the second −SH group is left dangling at the surface of the organic film and available to act as a binding site, for example, to a metal nanoparticle. This has been proposed as an interesting method to study the properties of isolated nanoparticles.[8] Regarding these and other applications, a major hurdle, as opposed to alkanethiols,[9−17] is the possibility that both thiol ends bind to the metal surface, instead of leaving one end free.[18−23] Frequently, mixed phases may result depending upon assembly conditions and there is an ongoing debate in the literature[18] about the possibility of obtaining ordered monolayer films of standing-up dithiol molecules. Despite many attempts, the conditions for the reproducible formation of highly ordered compact self-assembled monolayers (SAMs), with free −SH end groups at the outer interface, depending subtly on factors such as the quality of the substrate and reagents, solvent strength, photochemical action, and so forth were until recently not clearly defined.

Recently, some of us have shown that under specific assembly conditions,[19,20] that is, when dithiols were assembled in well

Received: December 22, 2010
Revised: February 24, 2011
Published: March 15, 2011

dx.doi.org/10.1021/la105063u | *Langmuir* 2011, 27, 4713–4720

degassed hexane and in the absence of light, well ordered films could be obtained. In the case of alkanedithiols, it was noted that the final quality of the desired upright configuration of molecules depended on chain length: short chain molecules such as butanedithiol tend to remain in a lying down configuration, whereas nonanedithiol was mostly standing up.

Molecules with aromatic rings have attracted particular attention[24−27] because of their conducting character, and in particular early measurements[28] of molecular resistance involved the use of a 1,4-benzenedimethanethiol (BDMT) molecule.

The present work arises from a collaboration between groups which have already investigated in some detail the formation of BDMT SAMs on well-defined gold surfaces exploiting both in-vacuum[29−31] and in-liquid deposition.[32,33] Regarding deposition from solution, a procedure that may be easier to implement in some applications, an initial study by some of us[32] surveyed the preparation of films in room temperature solutions of ethanol, methanol, and n-hexane. Measurements of X-ray absorption with linearly polarized light at the C 1s edge and photoemission from C 1s, Au 4f, and S 2p core levels were applied to investigate (i) the degree of coverage of the organic films; (ii) the molecular orientation at the surface; and (iii) the molecule/substrate chemical bonding. Photoemission experiments indicated that, under all the preparation conditions investigated, an effective thickness exceeding the monolayer was obtained.

More recently, BDMT SAMs in solution have been studied applying the same procedure used for alkanedithiols, using a properly N_2 degassed n-hexane solution heated to 60 °C and in the absence of light.[33] The SAMs were characterized by spectroscopic ellipsometry (SE), X-ray photoelectron spectroscopy (XPS), cyclic voltammetry (CV), and grazing incidence reflection adsorption infrared spectroscopy (RAIRS). This procedure showed the formation of well ordered monolayers as opposed to preparations which used hexane at room temperature and in preparations using ethanol.

Encouraged by the results obtained with the new deposition protocol in n-hexane,[33] we decided to perform a new detailed high resolution photoemission and near edge X-ray adsorption spectroscopy study in order to obtain information about the orientation of the molecules and other characteristics of the film such as valence band features. The results of these experiments unambiguously testifying to the excellent quality of SAMs obtained and assessing the molecular orientation are described in the following.

EXPERIMENTAL SECTION

SAM Preparation. We used 200 nm thick gold on mica substrates, bought from PHASIS. The substrates were annealed at 600 °C for 30 s in an oven, followed by cooling performed under a N_2 flow. Final rinsing was done with hexane before drying under N_2. This procedure as shown previously yields high quality substrates with large (micrometer sized) terraces, and a dielectric function derived from SE gave results in excellent agreement with literature.[15] BDMT (98% purity) was obtained from Aldrich and used without further purification.

The SAMs were prepared by immersing the gold support into a freshly prepared 1 mM solution of n-hexane for about 30 min at 60 °C. We used solutions freshly degassed by N_2 bubbling. The samples were then rinsed with the same (fresh) solvent of the solution and dried with N_2. To minimize photooxidation effects, all these procedures were carried out in absence of ambient light.

Photoemission. Experiments were performed at the BEAR beamline (Elettra synchrotron radiation laboratory, Trieste, Italy).[34] Photoemission measurements were performed with a hemispherical deflection analyzer (66 mm mean radius) driven at constant pass energy, with an overall energy resolution of <200 meV (analyzer and beamline). Spectra were recorded at normal emission, with the light impinging at 45° with respect to surface normal. We used $h\nu$ = 184 eV for Au 4f, $h\nu$ = 385 eV for C 1s, and $h\nu$ = 260 eV for S 2p levels. The photon energies were chosen in order to measure the photoelectron peaks of the different core levels approximately at the same final kinetic energies (E_k = 90−100 eV). These conditions were chosen in order to maximize the surface sensitivity, measuring photoelectrons with kinetic energies corresponding to the minimum of the inelastic mean free path ($\Lambda \sim 6$ Å).[32,35] Moreover, the use of lower photon energies with respect to the Al and Mg Kα lines, used in a previous experiment,[33] results in a higher photoabsorption cross section[36] for the different core levels of interest. The emission lines from Au 4f levels were acquired at each photon energy and were taken as an energy reference for the alignment of the spectra on the binding energy scale (Au $4f_{7/2}$ = 84.0 eV). The valence band of the system was also measured at normal emission and at 60 eV of photon energy.

Near Edge X-ray Absorption. The near edge X-ray absorption fine structure (NEXAFS) spectra were measured at the C 1s edge keeping fixed the incidence angle (8° with respect to surface plane) and varying the direction of the electric field vector from perpendicular to the scattering plane (s-incidence geometry) to parallel to it (p-incidence geometry). This was accomplished by rotating the experimental chamber around the beam axis by an angle Ψ_C, from Ψ_C = 0° (s-scattering) to 90° (p-scattering). This guarantees that the illuminated area and the incidence angle remain virtually unchanged for different angles Ψ_C. The synchrotron beam was elliptically polarized with its major electric field component oriented in the horizontal direction (H) of the laboratory, giving a photon ellipticity $\varepsilon = |\vec{E}_V|^2/|\vec{E}_H|^2$ of about 0.3 (ε = 1 for circularly polarized and ε = 0 for perfectly linearly polarized radiation). This was evaluated as a good compromise to distinguish linear dichroism effects without reducing the beam flux. Measurements were carried out by acquiring the drain current from the sample (total yield mode). The photon energy resolution was set at 0.1 eV. In order to take into account the incident flux fluctuations and to correct for their dependence on wavelength (source plus optics transmission), the absorption spectra were first normalized to the current drained by a gold mesh (flux monitor) and also normalized to a reference absorption spectrum taken under the same experimental conditions and energy range on a carbon free Au(111) surface. Characteristic features of the flux monitor signals were used for the alignment of the energy scale of the spectra. The spectra were first corrected for the Au absorption cross section, as calculated from the Henke tables,[37] then they were rescaled to the values derived from Henke at the carbon edge before and well above the edge region. Reproducibility was tested by taking multiple scans. All measurements were performed at room temperature.

THEORETICAL METHODS

The equilibrium geometry, electronic structure, and density of states (DOS) of a single molecule grafted on a Au cluster composed of 13 atoms were calculated by DFT with the computer code STOBE.[38] A gradient corrected RPBE exchange/correlation functional was applied.[39,40] To calculate the equilibrium geometry and the valence band properties, we used all-electron triple-valence plus polarization TZVP atomic Gaussian basis sets for sulfur and carbon centers, while a (311/1)-type basis set was chosen for the hydrogen sites.[41] For the Au cluster atoms, we used effective core potentials, describing the core and the appropriate valence basis.[38]

During the geometry optimization step the Au atoms of the cluster were kept at fixed positions relative to their bulk value. The degrees of freedom of the BDMT molecule were reduced, assuming chemisorption through one of the S atoms on the (111) oriented face of the Au cluster. Also the tilt angle of the molecular longitudinal axis relative to the surface normal was kept fixed at the experimental value of 24° obtained from NEXAFS (see below). The molecule was allowed to move vertically with respect to the Au surface and the angular orientation and position of the methylene CH_2 units were left free to vary. Different adsorption sites

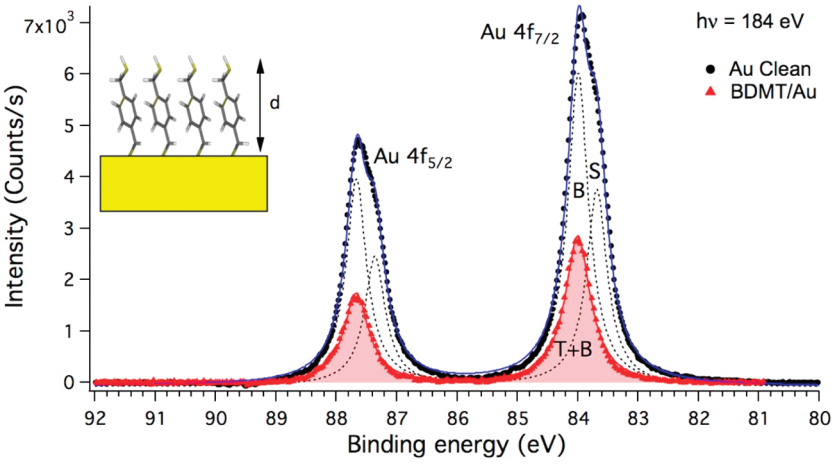

Figure 1. Comparison between the Au 4f levels before and after BDMT SAM formation (dots, experimental curves; lines, fit). Shaded areas (in red) correspond to the spectra taken after BDMT deposition. B indicates the bulk component, S the surface component of the clean substrate, and T the Au atoms bonded to thiolate species.

(hollow, bridge, and on top) were tested. The minimum total energy was obtained for chemisorption on the "on top" position. The starting configuration of the BDMT molecule was taken from ref 29. The final geometry (on top position) is shown in the inset of Figure 4 below.

RESULTS AND DISCUSSION

Photoemission. In Figure 1, the Au 4f spectra of the clean Au substrate and after the growth of the BDMT SAM are compared. The clean substrate spectrum refers to a sample that underwent the same annealing and cleaning procedure applied to the ones used for the organic film assembly. A shoulder of the main 4f doublet of the clean substrate spectrum is clearly evident toward the lower binding energies. For the treatment of the Au spectral components, we adopted the same procedure as in previous works on thiolate SAMs.[29,32] In brief, after normalization for the incoming photon flux and subtraction of a Shirley-like background, Voigt functions have been fitted to the photoemission peaks. The spectrum was fitted with two Voigt doublets, accounting for the 3.6 eV spin−orbit splitting of the 7/2 and 5/2 components, with overall widths of 0.3 eV. Regarding the bare substrate, the main component (B in Figure 1) is centered at 84.0 ± 0.1 eV and is associated to bulk Au. The component at 83.7 ± 0.1 eV (S in Figure 1) is associated with the reconstruction of surface atoms of the Au surface. This is consistent with previous results, as reported in literature.[44−46] After the formation of the BDMT film, a sizable decrease of the Au 4f photoemission intensity is observed. The corresponding spectrum has been fitted with a single Voigt doublet, which is centered at the bulk position of 84.0 ± 0.1 eV, with a full width at half-maximum (fwhm) of 0.4 eV. The increased width of the component with respect to B and S features of the clean spectrum can be associated to the presence of contributions from surface Au atoms interacting with a thiolate sulfur.[46−48] The resolution is not sufficient to disentangle unambiguously this contribution, even if a slight asymmetry is present in the spectrum toward the higher binding energy side of the peak. For this reason, we labeled the peak after BDMT adsorption as T+B in Figure 1, where T indicates thiolate induced contributions. It is noteworthy that the surface related component (S) of the clean gold is completely quenched upon adsorption, a characteristic which is common to alkanethiols on Au.[46,47]

Following a standard approach,[29,30,32] from the attenuation of the Au 4f spectra, it is possible to derive information on the effective film thickness, neglecting the optical adsorption of the film and reflectivity effects and assuming that the film is uniform in thickness and homogeneous. Considering an inelastic mean free path $\Lambda = 6 \pm 1$ Å for the Au photoelectrons at 100 eV of kinetic energy in the organic film matrix,[32,35] we obtained an effective thickness value $d = 6.5 \pm 2.5$ Å.

Clearly, the derivation of the effective thickness by photoemission is strictly dependent on the chosen elastic mean free path of the photoelectrons. This is not always straightforward to evaluate, especially at low kinetic energies. This makes it difficult sometimes to compare values obtained in different experiments. In a previous work by some of us,[32] the same experimental apparatus, experimental geometries, and conditions were used to derive the effective thickness of BDMT films prepared in solution for 24 h dipping time and at room temperature. In that case, using the same value of the inelastic mean free path, we obtained values in the range 11−14 Å, which was interpreted in terms of the formation of a not complete bilayer of molecules. The value obtained in the present work is sizeably lower, and it is compatible with a single layer of molecules standing upright.

The S 2p spectrum is reported in Figure 2 after normalization to the photon flux and background subtraction. This spectrum presents a signal/noise (s/n) ratio decisively better than the one we could obtain in a recent experiment on the same system using a conventional X-ray source.[33] The spectrum has been fitted with Voigt doublets. For each S 2p doublet, a 1.2 eV spin orbit splitting and a 2:1 branching ratio between the 3/2 and 1/2 components was adopted.[29,32,42,43]

The peaks within each doublet were assumed to have the same width. Each doublet was identified in terms of the position of the 3/2 peak. The main doublet at 163.3 ± 0.1 eV (S_2), with a fwhm of 0.8 eV, is associated to "unbound" sulfur, that is, sulfur which is not directly engaged in a thiolate molecule−surface interaction, as for example free thiol (SH) groups or S−S bonds.[29,32,43,49,50] The lower binding energy component at 162.0 ± 0.1 eV (S_1'), with a fwhm of 0.7 eV, is accompanied by a weak structure at 160.9 ± 0.1 eV (S_1'').

dx.doi.org/10.1021/la105063u |*Langmuir* 2011, 27, 4713–4720

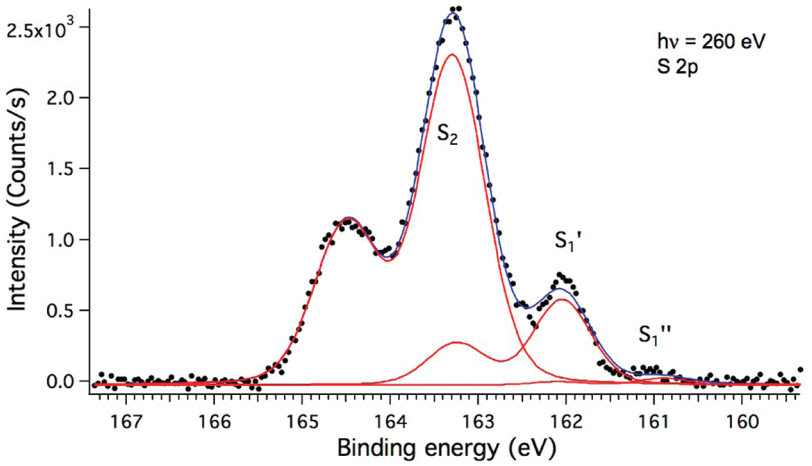

Figure 2. S 2p levels of BDMT film. The spectra are decomposed into three Voigt doublets. S_1' and S_1'' refer to interface sulfur, while S_2 is related to the "unbound" sulfur species.

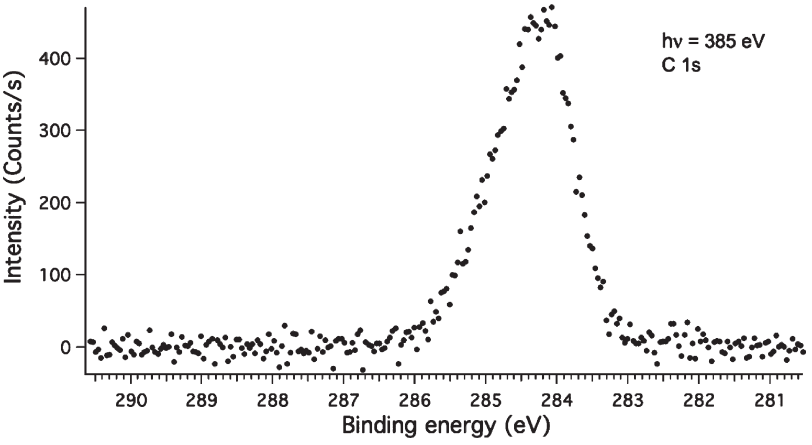

Figure 3. C 1s levels taken after BDMT film formation.

S_1' is assigned to thiolate sulfur bonding to the Au substrate. S_1'' could be associated with different bound configurations of the molecules to the substrate (different hybridization, adsorption site differences) or to atomic S, possibly due to some degree of irradiation induced damage.[29,32,42,43,49,51] Noticeably, the absence of high binding energy components (above 166 eV)[52,53] excludes the presence of oxidized sulfur species in the present SAM.

Insights on the formation of a compact monolayer can be obtained if one considers the S_2/S_1 (unbound/bound S) intensity ratio.[32,33] In the present case, this ratio is 4.1 ± 0.1, matching the value of 4 which is expected for a single layer of molecules standing upright[32,33] and sizeably less than the values (5.4−6.3) obtained for BDMT films prepared by dipping in different solvents for 24 h at room temperature.[32] This result, obtained on data of better quality than those of ref 33 (regarding the s/n ratio), indicates that the preparation method followed in the present study provides a single layer film, with the molecules assuming a vertical configuration.

In Figure 3, the C 1s photoemission peak is reported, after normalization to the photon flux and background subtraction. A single structure is observed, with a maximum at 284.2 ± 0.1 eV and with a slight asymmetry toward the high binding energy side. The main contribution to the photoemission peak at 284.2 eV can be associated to the aromatic C atoms and C atoms in the methylene units, while the high binding energy tail is related to shake-up processes due to the aromatic ring in the organic film.[29,30,32,49]

In Figure 4, the valence bands measured at a photon energy of 60 eV of the bare substrate and of the BDMT/Au system are compared. The spectra were taken in s-light polarization scattering conditions, that is, with the electric field vector parallel to the substrate plane. The clean gold spectrum is dominated by the emission from the 5d band of Au, extending from 2 to 8 eV of binding energy. The clean surface spectrum also exhibits sizable contributions from surface states of Au(111), just below the Fermi level (labeled Au SS) and at about 3 eV.[54]

After formation of the BDMT SAM, the characteristic features of the surface states of Au and some other features of the Au 5d band are strongly attenuated, while new features show up. They have been labeled from B_1 to B_7 in Figure 4. The difference spectrum is also reported, in which the spectral variations induced by the adsorbate are better emphasized. These features are associated to the different molecular orbital contributions.[29]

To help in a better assignment and to improve the results shown in ref 29, we calculated the DOS associated with the BDMT molecule chemisorbed on a Au cluster, as shown in the

dx.doi.org/10.1021/la105063u |*Langmuir* 2011, 27, 4713–4720

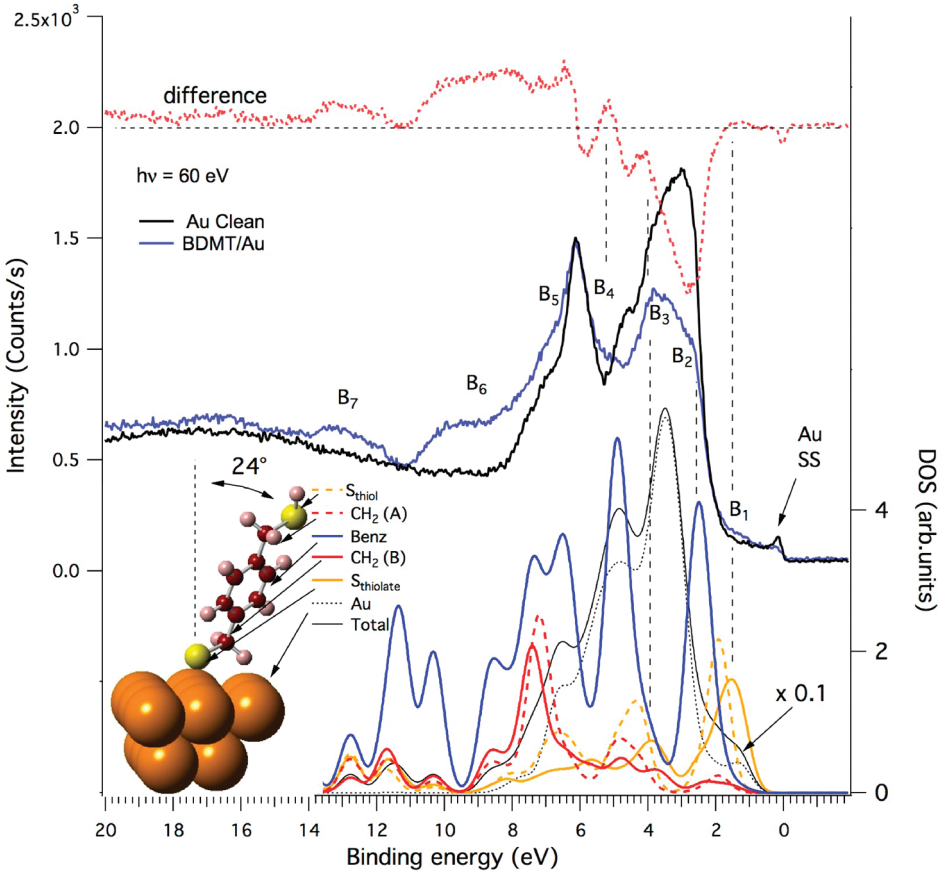

Figure 4. Top-left vertical scale: Valence band taken on the bare substrate (black) and after BDMT chemisorption (blue). The difference spectrum is also reported. Bottom-right vertical scale: DOS of BDMT on a Au cluster. The partial DOS projected on the different molecular sections is reported. Total DOS (black thin solid line) and Au cluster DOS (black thin dashed line) have been multiplied by a factor of 0.1 for better display of molecular induced states. CH_2 (A) and CH_2 (B) refer to the different methylene groups farther and closer to the substrate, respectively.

inset of Figure 4. Different partial DOS (PDOS) were calculated, projected on the different molecular sections, to disentangle their different contributions. The DOS in Figure 4 corresponds to the molecule adsorbed on an "on top" site, presenting the minimum of total energy as compared with adsorption on bridge or hollow sites. More complex configurations, as proposed for aliphatic SAMs, were not considered here.[55] Our main attention was to disentangle the contributions from the different molecular groups after adsorption with respect to the bare molecule.

For presentation purposes and to emphasize molecular features with respect to gold related structures, the total and the Au cluster partial DOS were multiplied by a factor of 0.1 in Figure 4. The calculated DOS was also shifted to align with the experimental spectra. It can be seen that, due to the loss of hydrogen and bonding to the Au cluster, the PDOS molecular contributions from the CH_2 and S head groups located symmetrically with respect to the benzene ring unit and which give identical contributions in the isolated symmetric BDMT molecule[29] are now split into separate structures. For example, the HOMO state, giving contributions to B_1 just below the Fermi energy and overlapping with the Au cluster states, is associated to the thiolate sulfur, while the unbound sulfur group contributes to the left side of the same feature B_1. Features B_2, B_4—B_7 are related to states mainly localized on the benzene ring. B_2 in particular is mostly related to the π-type states of benzene[29] and to a minor extent to unbound S and to S thiolate. This feature is not so evident in the difference spectrum, mainly due to the drastic decrease of the gold surface state at about 3 eV. S groups seem to contribute to feature B_3. Methylene units, together with the benzene ring, contribute principally to feature B_5—B_6, with the more external CH_2 group (A in Figure 4) weighing on the broad shoulder between B_5 and B_6. B_7 can be finally related to benzene ring states. We stress that the calculation refers to a single BDMT molecule onto an Au cluster. In this sense, interaction effects between adjacent chemisorbed molecules are not described by the calculation, which can be responsible for the differences with the experimental curve. Complex adsorption geometries involving Au adatoms[55] were not considered.

X-ray Absorption. NEXAFS spectra taken at the C1s edge as a function of the orientation angle of the electric field vector with respect to the surface plane are reported in Figure 5. NEXAFS spectroscopy is known to be a powerful tool in the investigation of organic molecules at surfaces. It provides unique information both on the empty orbitals of organic molecules and on their orientation with respect to the substrate.[56−58]

The spectra, whose features resemble those described previously,[29,32] were decomposed into individual Gaussian peaks and Gaussian-broadened step functions through a best-fitting procedure.[56] This permits us to identify the different electronic transitions from the C 1s core states to empty molecular levels. Best fit results are reported in Figure 5 only for the spectrum taken at $\Psi_C = 0°$ (s-scattering condition). Analogous results were obtained at

dx.doi.org/10.1021/la105063u |*Langmuir* 2011, 27, 4713–4720

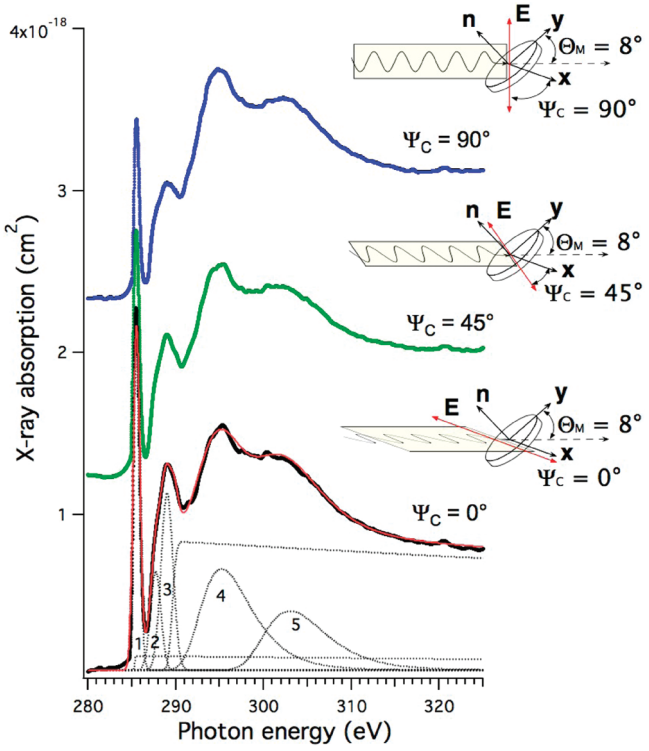

Figure 5. Near edge X-ray absorption spectra taken at different angles between the surface plane and the electric field vector. Dots, experimental data; continuous line, fit of the experimental curve taken at Ψ_C = 0°; dashed lines, asymmetric Gaussian and step functions used to fit the spectrum. The scattering geometry is reported for each curve: the incidence angle is kept fixed, while the plane of linear polarization of the light is rotated around the beam axis.

the other angles. Symmetric Gaussian peaks were used for the first three transitions, while asymmetric Gaussian peaks were used for the last two transitions, consistent with the analysis performed on BDMT films prepared in different solutions and from the vapor phase in our earlier works.[29,32]

On the basis of our previous findings[29,32] the first pronounced peak (1) at 285.5 eV is associated to the C=C/π^* resonance involving the C atoms of the aromatic ring; the second structure (2) at 287.7 eV is assigned to transitions involving the C atoms in the methylene units, and in particular to a C−S/σ^*-type resonance; the third structure (3) at 289.0 eV is related mainly to π^* excitations involving the aromatic ring atoms; and the fourth (4) and fifth (5) structures at 295.2 and 303.0 eV are assigned to C−C/σ^* and C=C/σ^* resonances. More precisely, contributions to the last two features mainly originate from the σ_1^* and σ_2^* resonances typical of the benzene ring.[59]

Two step functions were additionally used to properly fit the spectra. The first step at 285.4 eV is related to a partial interaction between the metal and the molecular π^* states, leading to electron excitation above the Fermi level of the substrate. This is also consistent with our DFT calculation, showing the LUMO state of the molecule to be highly interacting with the Au atoms of the cluster. The second step is located about 4.5 eV higher than the first step, and it is related to the excitation of the C 1s electrons into the continuum of empty states above the vacuum level. These transitions correspond to excited electrons in the molecule that present no or negligible projection onto the metallic bands.

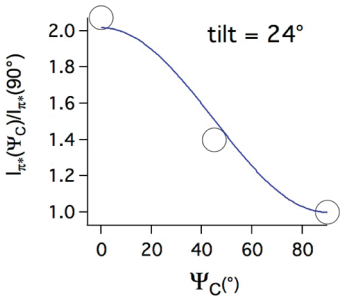

Figure 6. π^* intensity measured at different Ψ_C angles and normalized to the intensity of the π^* transitions at Ψ_C = 90°.

Following the angular dependence of the most intense feature (1), it was possible to derive information on the average orientation of the molecules. From first inspection of the experimental curves in Figure 5, it can be noticed that the intensity of feature (1) is progressively reduced when the polarization vector passes from s- to p-light scattering conditions. This supports the idea of an upward orientation of the BDMT molecules.

To estimate quantitatively the average orientation of the molecular plane with respect to the surface plane, we monitored the angular dependence of the π^* resonance (feature 1). In Figure 6, we show the behavior of the π^* intensity measured at different Ψ_C angles and normalized to the intensity of the π^* transition at Ψ_C = 90°.

For ternary symmetry surfaces (111 surfaces with possibly three domains), the intensities can be fitted with the following relation[60]

$$\frac{I_{\pi^*}(\theta)}{I_{\pi^*}(90°)} = \frac{A\pi(\sin^2\theta_M \sin^2\theta + 2\cos^2\theta_M \cos^2\theta) + B\pi \sin^2\theta}{A_{(\Psi_C=90°)}\pi(\sin^2\theta_M \sin^2\theta + 2\cos^2\theta_M \cos^2\theta) + B_{(\Psi_C=90°)}\pi \sin^2\theta}$$

where θ_M is the grazing incidence angle (8° in our case), θ is the angle between the direction of the dipole moment associated to the transition and the surface normal (to be determined), and

$$A = \varepsilon^2 \cos^2\psi_C + \sin^2\psi_C - 2\varepsilon \cos\psi_C \sin\psi_C \cos\delta$$
$$B = \cos^2\psi_C + \varepsilon^2 \sin^2\psi_C + 2\varepsilon \cos\psi_C \sin\psi_C \cos\delta$$

with δ being the phase difference between the vertical and horizontal components of the electric field vector (90° in our case) and ε the photon ellipticity. The θ angle, which in our case is represented by the angle between the normal to the benzene ring plane and the surface normal, was left as a free fit parameter. The best fit result indicates an average tilt angle of the benzene ring normal of 66° ± 2° with respect to the surface normal; this in turn suggests that the longitudinal axis of the molecule is tilted by 24° ± 2° with respect to the surface normal, as represented in the inset of Figure 4. In ref 32, we observed average angles of the order of 28−31° for BDMT films prepared in ethanol, methanol, and n-hexane for 24 h. The results obtained here demonstrate further that the present preparation procedure gives rise to good quality SAMs, in terms of the alignment of the molecules along the vertical direction.

CONCLUSIONS

We reported a study of the self-assembly of 1,4-benzenedimethanethiol monolayers on gold formed according to a recently devised procedure.[33] In this work, the valence band characteristics, the thickness of the layer, and the orientation of the molecules were

dx.doi.org/10.1021/la105063u |Langmuir 2011, 27, 4713–4720

analyzed using photoelectron spectroscopy with synchrotron radiation and near edge X-ray absorption spectroscopy. These measurements, together with previous RAIRS, XPS, and ellipsometry results,[33] unambiguously attest the formation of a single molecular layer with molecules arranged in the upright position and presenting a free −SH group at the SAM−air interface. XAS measurements indicate that the molecular axis is oriented at 24° to the surface normal. In addition, valence band features could be successfully associated to specific molecular orbital contributions thanks to the comparison with theoretically calculated density of states projected on the different molecular units.

AUTHOR INFORMATION

Corresponding Author

*E-mail: vladimir.esaulov@u-psud.fr.

ACKNOWLEDGMENT

We acknowledge financial assistance from the European Community, the Triangle de la Physique, the France-India Ile de France ARCUS project, The France-Italy CNRS PICS agreement, and Sincrotrone Trieste. The authors are grateful to Drs. O. Cavalleri and M. Prato for useful discussions. The BEAR beamline staff is gratefully acknowledged for technical assistance during the measurements.

REFERENCES

(1) Andres, R. P.; Bein, T.; Dorogi, M.; Feng, S.; Henderson, J. I.; Kubiak, C. P.; Mahoney, W.; Osifchin, R. G.; Reifenberger, R. *Science* **1996**, 1323–1325.

(2) Käshammer, J.; Wohlfart, P.; WeiB, J.; Winter, C.; Fisher, R.; Mittler-Neher, S. *Opt. Mater.* **1998**, *9*, 406–410.

(3) Sakotsubo, Y.; Ohgi, T.; Fujita, D.; Ootuka, Y. *Phys. E* **2005**, *29*, 601–605.

(4) Vijaya Sarathy, K.; John Thomas, P.; Kulkarni, G. U.; Rao, C. N. R. *J. Phys. Chem. B* **1999**, *103*, 399–401.

(5) Rieley, H.; Kendall, G. K.; Zemicael, F. W.; Smith, T. L.; Yang, S. *Langmuir* **1998**, *14*, 5147–5153.

(6) Aliganda, A. K. A.; Lieberwirth, I.; Glasser, G.; Duwez, A.-S.; Sun, Y.; Mittler, S. *Org. Electron.* **2007**, *8*, 161–174.

(7) Garcia-Raya, D.; Madueo, R.; Blàzquez, M.; Pineda, T. *Langmuir* **2010**, *26* (14), 11790–11796.

(8) Ohgi, T.; Sheng, H.-Y.; Nejoh, H. *Appl. Surf. Sci.* **1998**, *130−132*, 919–924.

(9) Love, J. C.; Estroff, L. A.; Kriebel, J. K.; Nuzzo, R. G.; Whitesides, G. M. *Chem. Rev.* **2005**, *105*, 1103–1169.

(10) Porter, M. D.; Bright, T. B.; Allara, D. L.; Chidsey, C. E. D. *J. Am. Chem. Soc.* **1987**, *109*, 3559–3568.

(11) Laibinis, P. E.; Whitesides, G. M.; Allara, D. L.; Tao, Y.-T.; Parikh, A. N.; Nuzzo, R. G. *J. Am. Chem. Soc.* **1991**, *113*, 7152–7167.

(12) Jung, Ch.; Dannenberger, O.; Xu, Y.; Buck, M.; Grunze, M. *Langmuir* **1998**, *14* (5), 1103–1107.

(13) Guo, Z.; Zheng, W.; Hamoudi, H.; Dablemont, C.; Esaulov, V. A.; Bourguignon, B. *Surf. Sci.* **2008**, *602*, 3551–3559.

(14) Subramanian, S.; Sampath, S. *J. Ind. Inst. Sci.* **2009**, *89*, 1–7.

(15) Prato, M.; Moroni, R.; Bisio, F.; Rolandi, R.; Mattera, L.; Cavalleri, O.; Canepa, M. *J. Phys. Chem. C* **2008**, *112*, 3899–3906.

(16) Tai, Y.; Shaporenko, A.; Rong, H.-T.; Buck, M.; Eck, W.; Grunze, M.; Zharnikov, M. *J. Phys. Chem. B* **2004**, *108*, 16806–16810.

(17) Noh, J.; Kato, H. S.; Kawai, M.; Hara, M. *J. Phys. Chem. B* **2006**, *110* (6), 2793–2797.

(18) Liang, J.; Rosa, L. G.; Scoles, G. *J. Phys. Chem. C* **2007**, *111*, 17275–17284.

(19) Hamoudi, H.; Guo, Z. A.; Prato, M.; Dablemont, C.; Zheng, W. Q.; Bourguignon, B.; Canepa, M.; Esaulov, V. A. *Phys. Chem. Chem. Phys.* **2008**, *10*, 6836–6841. Hamoudi, H.; Dablemont, C.; Esaulov, V. A. *Surf. Sci.* **2011**, *605*, 116.

(20) Daza Milone, M. A.; Hamoudi, H.; Rodríguez, L. M.; Rubert, A.; Benitez, G. A.; Vela, M. E.; Salvarezza, R. C.; Gayone, J. E.; Sánchez, E. A.; Grizzi, O.; Dablemont, C.; Esaulov, V. A. *Langmuir* **2009**, *25*, 12945–12953.

(21) Garca-Raya, D.; Madueo, R.; Blàzquez, M.; Pineda, T. *J. Phys. Chem. C* **2010**, *114* (8), 3568–3574.

(22) Carot, M. L.; Esplandiu, M. J.; Cometto, F. P.; Patrito, E. M.; Macagno, V. A. *J. Electroanal. Chem.* **2005**, *579*, 13–23.

(23) Franke, A.; Pehlke, E. *Phys. Rev. B* **2010**, *81*, 075409.

(24) Zharnikov, M.; Frey, S.; Rong, H.; Yang, Y. J.; Heister, K.; Buck, M.; Grunze, M. *Phys. Chem. Chem. Phys.* **2000**, *2*, 3359–3362.

(25) Rong, H.-T.; Frey, S.; Heister, K.; Yang, Y.-J.; Buck, M.; Zharnikov, M. *Langmuir* **2001**, *17*, 1582–1593.

(26) Azzam, W.; Cyganik, P.; Witte, G.; Buck, M.; Wöll, C. *Langmuir* **2003**, *19*, 8262–8270.

(27) Shaporenko, A.; Brunnbauer, M.; Terfort, A.; Grunze, M.; Zharnikov, M. *J. Phys. Chem. B* **2004**, *108*, 14462–14469.

(28) Andres, R. P.; Bein, T.; Dorogi, M.; Feng, S.; Henderson, J. I.; Kubiak, C. P.; Mahoney, W.; Osifchin, R. G.; Reifenberger, R *Science* **1996**, *272*, 1323.

(29) Pasquali, L.; Terzi, F.; Seeber, R.; Doyle, B. P.; Nannarone, S. *J. Chem. Phys.* **2008**, *128*, 134711.

(30) Pasquali, L.; Terzi, F.; Zanardi, C.; Seeber, R.; Mahne, N.; Nannarone, S.; Phys., J. *Cond. Matt.* **2007**, *19*, 305020.

(31) Alarcon, L. S.; Chen, L.; Esaulov, V. A.; Gayone, J. E.; Snchez, E. A.; Grizzi, O. *J. Phys. Chem. C* **2010**, *114*, 19993–19999.

(32) Pasquali, L.; Terzi, F.; Zanardi, C.; Pigani, L.; Seeber, R.; Paolicelli, G.; Suturin, S. M.; Mahne, N.; Nannarone, S. *Surf. Sci.* **2007**, *601*, 1419–1427.

(33) Hamoudi, H.; Prato, M.; Dablemont, C.; Cavalleri, O.; Canepa, M.; Esaulov, V. A. *Langmuir* **2010**, *26*, 7242–7247.

(34) Nannarone, S.; Borgatti, F.; De Luisa, A.; Doyle, B.P.; Gazzadi, G.C.; Giglia, A.; Finetti, P.; Mahne, N.; Pasquali, L.; Pedio, M.; Selvaggi, G.; Naletto, G.; Pelizzo, M.G.; Tondello, G. *AIP Conf. Proc.* **2004**, *705*, 450.

(35) Lamont, C. L. A.; Wilkes, J. *Langmuir* **1999**, *15*, 2037.

(36) Yeh, J. J.; Lindau, I. *Atomic Calculation of Photoionization Cross-Sections and Asymmetry Parameters*; Gordon and Breach Science Publishers: New York, 1993.

(37) Henke, B. L.; Gullikson, E. M.; Davis., J. C. *At. Data Nucl. Data Tables* **1993**, *54*, 181–342.

(38) STOBE-DEMON version 3.0, 2007, written by Hermann, K.; Pettersson, L. G. M.; Casida, M. E.; Daul, C.; Goursot, A.; Koester, A.; Proynov, E.; A. St-Amant, Salahub, D. R.; , Contributing authors: Carravetta, V.; Duarte, H.; Friedrich, C.; Godbout, N.; Guan, J.; Jamorski, C.; Leboeuf, M.; Leetmaa, M.; Nyberg, M.; Patchkovskii, S.; Pedocchi, L.; Sim, F.; Triguero, L.; , Vela, A.;

(39) Hammer, B.; Hansen, L. B.; Nørskov, J. K. *Phys. Rev. B* **1999**, *59*, 7413.

(40) Perdew, J. P.; Burke, K.; Ernzerhof, M. *Phys. Rev. Lett.* **1996**, *77*, 3865.

(41) Godbout, N.; Salahub, D. R.; Andzelm, J.; Wimmer, E. *Can. J. Chem.* **1992**, *70*, 560.

(42) Cavalleri, O; Gonella, G; Terreni, S; Vignolo, M; Pelori, P; Floreano, L; Morgante, A; Canepa, M; Rolandi, R. *J. Phys.: Condens. Matter* **2004**, *16*, S2477–S2482.

(43) Gonella, G.; Terreni, S.; Cvetko, D.; Cossaro, A.; Mattera, L.; Cavalleri, O.; Rolandi, R.; Morgente, A.; Floreano, L.; Canepa, M. *J. Phys. Chem. B* **2005**, *109*, 18003–18009.

(44) Heimann, P.; van der Veen, J. F.; Eastman, D. E. *Solid State Commun.* **1981**, *38*, 595.

(45) Heister, K.; Zharnikov, M.; Grunze, M.; Johansson, L. S. O. *J. Phys. Chem. B* **2001**, *105*, 4058.

(46) Tanaka, A.; Imamura, M.; Yasuda, H. *Phys. Rev. B* **2006**, *74*, 113402.

(47) Chaudhuri, A.; Lerotholi, T. J.; Jackson, D. C.; Woodruff, D. P.; Dhanak, V. *Phys. Rev. Lett.* **2009**, *102*, 126101.
(48) Cossaro, A.; Floreano, L.; Verdini, A.; Casalis, L.; Morgante, A. *Phys. Rev. Lett.* **2009**, *103*, 119601.
(49) Pugmire, D. L.; Tarlov, M. J.; Van Zee, R. D.; Naciri, J. *Langmuir* **2003**, *19*, 3720–3726.
(50) Lindberg, B. J.; Hamrin, K.; Johansson, G.; Gelius, U.; Fahlman, A.; Nordling, C.; Siegbahn, K. *Phys. Scr.* **1970**, *1*, 286–298.
(51) Himmelhaus, M.; Gauss, I.; Buck, M.; Eisert, F.; Wöll, Ch.; Grunze, M. *J. Electron Spectrosc. Relat. Phenom.* **1998**, *92*, 139.
(52) Duwez, A.-S. *J. Electron Spectrosc. Relat. Phenom.* **2004**, *134*, 97.
(53) Azzam, W.; Wehner, B. I.; Fischer, R. A.; Terford, A.; Wöll, C. *Langmuir* **2002**, *18*, 7766.
(54) Zimmer, H.-G.; Goldmann, A.; Courths, R. *Surf. Sci.* **1986**, *176*, 115.
(55) Chesneau, F.; Zhao, J.; Shen, C.; Buck, M.; Zharnikov, M. *J. Phys. Chem. C* **2010**, *114*, 7112.
(56) Stöhr, J. *NEXAFS Spectroscopy*; Springer Series in Surface Science; Springer: Berlin, 1992; Vol. 25.
(57) Fisher, D.; Marti, A.; Hähner, G. *J. Vac. Sci. Technol., A* **1997**, *15*, 2173.
(58) Stöhr, J.; Outka, D. A. *Phys. Rev. B* **1987**, *36*, 7891.
(59) Horsley, J. A.; Stöhr, J.; Hitchcock, A. P.; Newbury, D. C.; Johnson, A. L.; Sette, F. *J. Chem. Phys.* **1985**, *83*, 6099.
(60) Serkovic Loli, L.; Hamoudi, H.; Gayone, J.; Martiarena, M. L.; Sanchez, E. A.; Grizzi, O.; Pasquali, L.; Nannarone, S.; Doyle, B.; Dablemont, C.; Esaulov, V. A. *J. Phys. Chem. C* **2009**, *113*, 17866–17875.